

Conductivity properties of hollow ZnFe_2O_4 nanofibers doped polyaniline nanocomposites

R. D. Balikile¹ · Aashis S. Roy² · S. C. Nagaraju^{1,3} · G. Ramgopal⁴

Received: 2 January 2017 / Accepted: 17 January 2017 / Published online: 8 February 2017
© Springer Science+Business Media New York 2017

Abstract Zinc ferrite nanofibers doped polyaniline (PANI) nanocomposites have been prepared by oxidation polymerization technique in various weight percentages. The prepared nanocomposites were characterized by Fourier transmission infrared spectroscopy, X-ray's diffraction for structural studies, scanning electron microscopy and transmission electron microscopy for surface morphology. Further the composites are used for dielectric studies by two probe method using Keithley source meter. Among all nanocomposites, 15 wt% of PANI– ZnFe_2O_4 nanocomposite shows high conductivity 1.23 S/cm and lowest relaxation time of 0.021 μs in comparison to other compositions. The dielectric constant decreases as a function of applied frequency due to the multiple polarizations which occurs in polymer nanocomposite. The tangent loss decreases with increase in 15 wt% of filler up to 10^4 Hz after that it remains constant. Therefore these composites are suitable for electronic applications such as lossless materials, capacitor, sensors etc.

1 Introduction

Nanomaterials have a significant important role in the advancement of new polymeric nanocomposites that has ability to combine and improve both the physical and chemical properties with desired characteristics required for technological applications [1–3]. Semiconducting nanoparticles have several advantages due to superior transparency, electron mobility, wide band gap at 300 K and good thermal, electrical and optical properties [4]. H. K. Maleh and his coworkers studied very extensively and reported the several transition nanoparticles and nanoferrites that employed for electrochemical device, biosensors, biomarkers, nano-catalysts and optoelectronic devices [5–7]. The features of conducting polymer such as high air and thermal stability, facile synthesis, electrochemical properties, bio-compatibility, tunable electrical conductivity, reversibility, switching capability between conducting-oxidized and insulating reduced state is the basis of tremendous technological applications [8, 9]. The inorganic fillers at nanoscale exhibit high surface–volume ratio, and thus are expected to modify drastically the electrical, optical and magnetic properties of polymer nanocomposites. In general, the synthesis of a hybrid polymer inorganic material aims to obtain a new composite material with synergetic or complementary behaviors between the polymer and inorganic material. Polyaniline (PANI) is a most suitable polymer because of its relative ease in preparation, good environmental stability [10, 11] and tunable conductivity.

The understanding of charge transport mechanism in the nanocomposite materials is very important both from fundamental and technological point of view. The impedance measurement is one of the powerful techniques to characterize and realize the charge transport phenomenon in the complex nano system. Various theoretical models

✉ G. Ramgopal
dr_gramgopal@yahoo.co.in

¹ R&D, Bharathiar University, Coimbatore, Tamil Nadu, India

² Department of Industrial Chemistry, Addis Ababa Science & Technology University, Addis Ababa, Ethiopia

³ Department of Physics, Vidyavahini College, Tumkur, Karnataka, India

⁴ Department of Physics, Maharani's Science College, Bangalore, Karnataka, India

were developed for the description of charge transport in conducting polymers [12–14]. In spite of high doping of polymer, the charge carriers seems to be localized, so they should move in the material by hopping over or tunneling through the potential barriers between the localized states. Variable range hopping (VRH) [15] is the most common charge transport mechanism, this model assumes that carriers tunnel through the energy barriers between the localized states with the help of phonon thermal energy. 3D-VRH occurs in disordered polymers with structures similar to the amorphous semiconductors, where charges can choose a most easy path in any direction. Quasi-1D VRH occurs in the polymers where charges move along the polymer chain, with sudden inter-chain hopping [16–18]. In some cases polymerization and protonation leads to creation of small conducting islands distributed in non-conductive matrix. In such case charges, tunnel between these regions take place according to charged energy limited tunneling mechanism [19, 20]. Zinc ferrite (ZnFe_2O_4) has high refractive index, high electron mobility and direct band gap semiconductor with a band gap of 2.42 eV [21]. In polymer–metal oxide nanocomposite, conductivity depends on several factors such as oxidant to monomer ratio, percolation limit, surface morphology, size distribution, compactness and interfacial interactions between nanofibers and host matrix [22].

In this present work, author reports the preparation PANI, ZnFe_2O_4 nanofibers and PANI/ ZnFe_2O_4 nanocomposites via chemical oxidation method. The synthesized materials are characterized by Fourier transmission infrared spectroscopy (FTIR), X-ray's diffraction (XRD) techniques for structural studies and surface morphology by scanning electron microscopy (SEM) and transmission electron microscopy (TEM). Further the dielectric properties of the PANI and PANI/ ZnFe_2O_4 nanocomposites were investigated using Hioki LCR Q meter with two probe techniques.

2 Experimental details

2.1 Materials and method

Aniline, hydrochloric acid, ammonium persulphate, zinc sulphate ($\text{ZnSO}_4 \cdot 7\text{H}_2\text{O}$), ferrous sulphate ($\text{FeSO}_4 \cdot 7\text{H}_2\text{O}$), ferric chloride (FeCl_3), acetone, sodium hydroxide all chemicals used in this work were of AR grade and used as received without further purification. Ultra fine deionized water was used throughout the experiment.

2.2 Nanofibers synthesis

Zinc ferrite (ZnFe_2O_4) nanofibers were prepared by co-precipitation method [23] by taking high-purity $\text{ZnSO}_4 \cdot 7\text{H}_2\text{O}$, $\text{FeSO}_4 \cdot 7\text{H}_2\text{O}$ and FeCl_3 as starting materials. According to

the chemical formula each starting material was weighed separately, followed by addition of suitable quantity of de-ionized water to make them 0.5 M solutions and then mixed all these cationic solutions with constant stirring for complete dissolution. The NaOH solution was prepared in sufficient quantity at 1 M concentration and heated to 60 °C. Then, the heated NaOH solution was added drop wise into the cationic solution with constant stirring as well as heating till the precipitation occurred. Further heating of the precipitate in its alkaline condition was continued to a soaking temperature of 100 °C for 30 min in order to complete the reaction and stirring was maintained further for 6 h for ageing finally the obtained precipitated particles were washed with double distilled water and filtered several times before drying them at 60 °C for 12 h. The co-precipitated ferrite agglomerates was then grinded using agate mortar and pestle to obtain very fine fibers. These fibers were calcinated in silica crucible at 400 °C for further crystallization [24–26].

2.3 Synthesis of PANI/ ZnFe_2O_4 nanocomposites

0.1 M aniline was dissolved in 1 M hydrochloric acid and to this a known amount of ZnFe_2O_4 (5, 10, 15, 20 and 25 wt%) has added and stirred for 20 min to form metal oxide suspended in aniline hydrochloride. The above solution has refluxed for 3 h at 0–5 °C with 1 ml of camphor sulphonic acid which acts as a surfactant. Further, 0.1 M of ammonium persulphate [$(\text{NH}_4)_2\text{S}_2\text{O}_8$] which acts as the oxidant has added to the refluxed solution drop wise with continuous stirring for 6 h at ice temperature and allowed to keep 24 h without stirring for the completion of polymerization [27]. The resulting precipitate powder of PANI– ZnFe_2O_4 nanocomposite was obtained by using vacuum filtration and then washed with 0.1 HCl in order to remove the excess chlorine ions followed by water and acetone to remove the excess ammonium persulphate and unreacted monomers from the nanocomposites. Finally the resultant precipitate was dried under dynamic vacuum for 24 h to achieve a constant weight.

2.4 Characterization

The Perkin Elmer (model 783) IR spectrometer in KBr medium at room temperature was used to study the FTIR spectra of PANI and PANI– ZnFe_2O_4 nanocomposites. For recording FTIR spectra, sample powders were mixed with KBr in the ratio of 1:25 by weight and grounded to ensure the uniform dispersion of samples in KBr pellets. Approximately 1 mm thickness clean disc were prepared using a cylindrical dye.

The XRD patterns of the prepared samples were obtained by using Phillips X-ray diffractometer with Cu K α

radiation ($\lambda=1.5406 \text{ \AA}$). The diffractograms were recorded in terms of 2θ in the range $10^\circ\text{--}80^\circ$ with a scanning rate of $2^\circ/\text{min}$.

The surface morphology of PANI and its nanocomposites were studied by using Phillips SEM of model XL30 ESEM which is used to analyze the surface morphology. The prepared nanofibers were dispersed on the surface of carbon tape which is mounted on an aluminum tab and to avoid charging on the surface of the samples a conducting gold is sputtered then the selected areas were photographed. A Hitachi H-7000 TEM operated at 100 kV and $\sim 30 \mu\text{A}$ was used to observe TEM images of synthesized ZnFe_2O_4 and PANI- ZnFe_2O_4 nanocomposites.

The electrical studies are measured by a Kelvin two probe method. Pure PANI and the PANI/ ZnFe_2O_4 nanocomposites at different % loadings were crushed into fine powder in an agate mortar in acetone medium. The nanocomposite powder was pressed in the form of pellets of 10 mm diameter and thickness which varied by 1 mm. The electrical measurements on these samples were made by applying the silver paste on either side for better contact.

3 Results and discussion

Figure 1 represents the FTIR spectra of (a) pure PANI, (b) ZnFe_2O_4 nanofibers and (c) 15 wt% of ZnFe_2O_4 doped PANI nanocomposites. The spectrum PANI observed the band at 1546 cm^{-1} and a weak band at 1478 cm^{-1} are

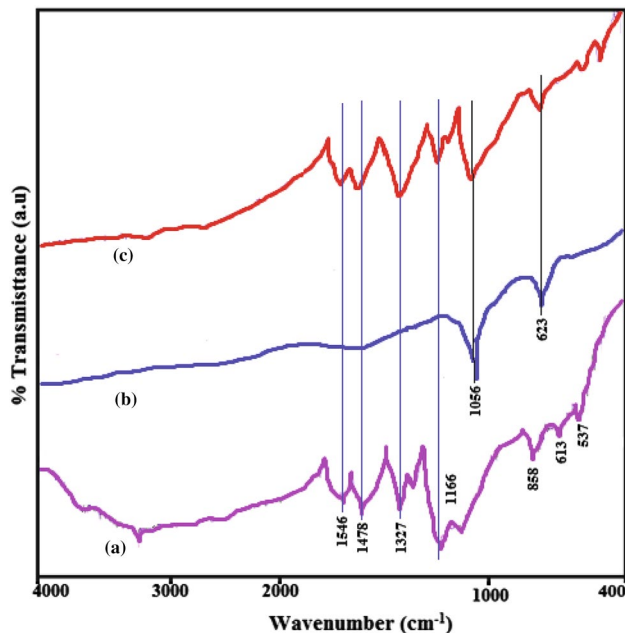


Fig. 1 FTIR spectra of (a) PANI, (b) ZnFe_2O_4 and (c) 15 wt% of PANI/ ZnFe_2O_4 nanocomposites

assigned to stretching vibration of C=C and C–C in the benzenoid ring and quinoid ring, respectively. The absorption at 1327 cm^{-1} corresponds to C–H in-plane deformation modes, 1166 and 858 cm^{-1} for C–N and C–H stretching vibration of aromatic ring respectively, 613 and 537 cm^{-1} are due to the bending out of the plan [28–30]. In FTIR spectrum of ZnFe_2O_4 nanofibers shows the strong absorption band of tetrahedral peaks at 623 cm^{-1} is due to Zn–O stretch vibrations and octahedral peaks at 1056 due to O–Fe–O bending out of the plan. All the characteristics peaks of ZnFe_2O_4 are reappeared without any shift in the 15 wt% of PANI/ ZnFe_2O_4 nanocomposites spectra confirm the formation of nanocomposites [31].

Figure 2 shows the XRD pattern of (a) polyaniline, (b) ZnFe_2O_4 , (c, d) 5 and 15 wt% of ZnFe_2O_4 hollow fibers in PANI nanocomposites. It is evident from the Fig. 2a that, the pure polyaniline has broad peak in the region of 26.4° indicating its semicrystalline nature. The diffraction pattern for ZnFe_2O_4 nanofibers (Fig. 2b) shows a cubic structure in spinel phase with fcc structure (JCPDS card no. 82-1042) with no extra reflections and are well indexed to the crystallographic planes of (220), (311), (222), (400), (422), (511), and (440) which corresponds to the diffraction in XRD at 26.5° , 34.8° , 36.8° , 44.8° , 54.3° , 57.6° and 63.4° with 100% intensity at 34.87° that corresponds to the reflection plane (311). The average particle size was determined by Debye–Scherrer’s formula and for pure ZnFe_2O_4 it is found to be 20 nm. In the Fig. 2b, c shows the 5 and 15 wt% of ZnFe_2O_4 hollow fibers in PANI. It is observed that the increasing in content of ZnFe_2O_4 nanofibers in the nanocomposite the relative intensity of the characteristic peaks of PANI/ ZnFe_2O_4 composites increase regularly, clearly indicating an increase in the ZnFe_2O_4 content in nanocomposites [32].

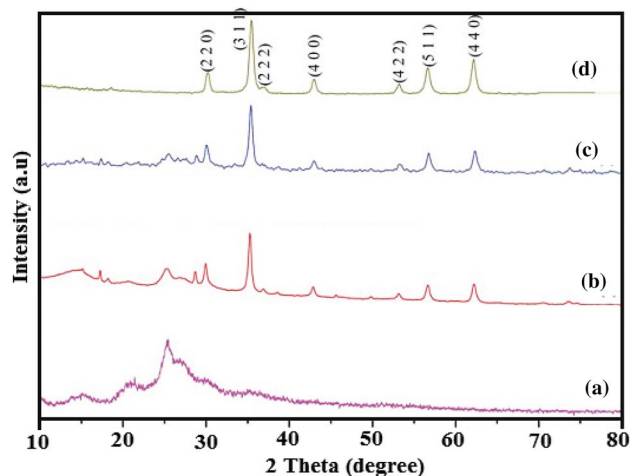


Fig. 2 XRD pattern of (a) PANI, (b) ZnFe_2O_4 and (c, d) 5 and 15 wt% of PANI/ ZnFe_2O_4 nanocomposites

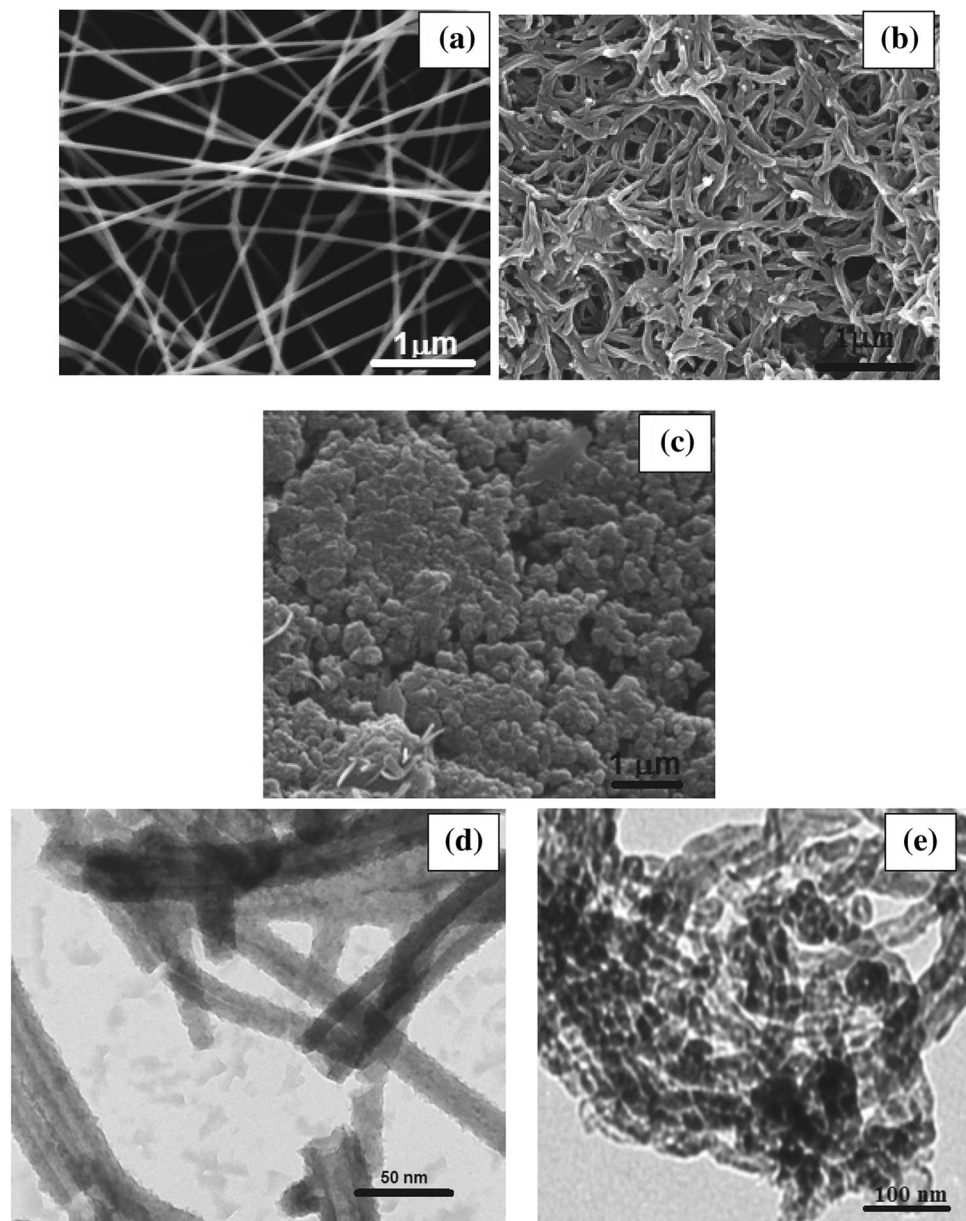
The morphologies of pure PANI and PANI/ZnFe₂O₄ nanocomposite are investigated by a SEM and TEM shown in Fig. 3. Figure 3a shows the SEM of pure PANI, a typical long fiber like structure can be observed with a uniform fiber size distribution. In Fig. 3b shows the SEM image of 15 wt% of ZnFe₂O₄ doped PANI nanocomposites and it is observed that the polymers were coated over the zinc ferrite fibers uniformly throughout the matrix. It is interesting to note that the zinc ferrite particles are not found on the surface of fibers may be due to the hollow nature of nanocomposites. Figure 3c shows the 20 wt% of PANI/ZnFe₂O₄ nanocomposite, it is observed that the ferrite fibers are not homogeneously distributed and gains are highly agglomerated to form a bundle. It is also important to notice that zinc

ferrite is embedded within the PANI matrix. Figure 3d, e shows the TEM image of pure ZnFe₂O₄ fibers and 15 wt% of PANI nanocomposites. When the aniline polymerized by oxidation methods it grown on the fiber surface in such away form one-dimensional structure as shown in Fig. 3e.

4 DC conductivity

Figure 4 shows the DC conductivity of PANI and its nanocomposites against temperature with various weight percentages such as 5, 10, 15, 20 and 25 wt% of ZnFe₂O₄ in PANI. It is observed that the conductivity increase with increase in temperature as well as weight percentage of up

Fig. 3 SEM image of **a** ZnFe₂O₄, **b** 15 wt% of PANI/ZnFe₂O₄, **c** 20 wt% of PANI/ZnFe₂O₄ nanocomposites, **d** TEM image of ZnFe₂O₄ and **e** 15 wt% of PANI/ZnFe₂O₄ nanocomposites



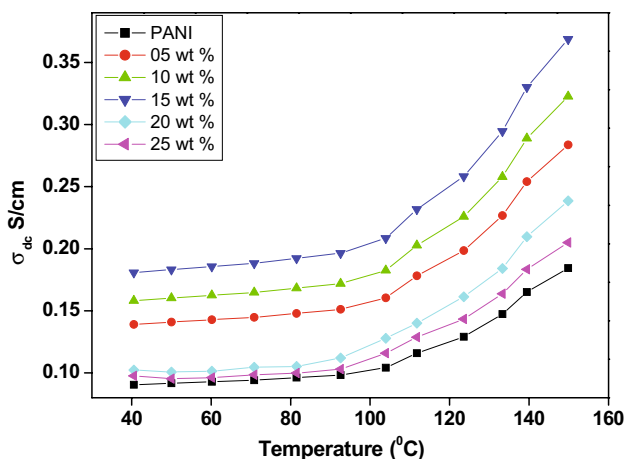


Fig. 4 DC conductivity of polyaniline and PANI–ZnFe₂O₄ nanocomposites for 5, 10, 15, 20 and 25 wt% by doping ZnFe₂O₄ in polyaniline

to 15 wt% of ZnFe₂O₄ in PANI after which the conductivity decreases. The increase in conductivity due to the extending of polymer chain due to the thermal energy and the hopping of charge carriers from low energy level to high energy level and the decrease in conductivity after 15 wt% is due to blocking of the charge carriers at the interface. Among all nanocomposites, 15 wt% shows high conductivity of 0.35 S/cm having lowest activation energy and extending of polymer nanocomposites. The above 15 wt% of nanocomposites showing the decrease in conductivity is due to the blocking of charge carriers at the interface of the agglomerated grains of the nanocomposites as shown in the 20 wt% of SEM image. The extending of polymer chain length can be confirmed by negative thermal coefficient (NTC) as shown in Fig. 5. It is observed that the polymer

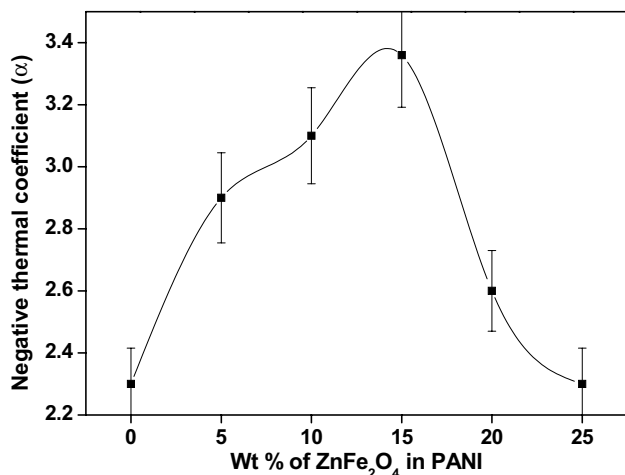


Fig. 5 NTC of polyaniline and 5, 10, 15, 20 and 25 wt% by doping ZnFe₂O₄ in polyaniline

nanocomposites chain length increase with increase in thermal energy up to 15 wt% of about 3.4 after which the decrease in value may be due to the high percentages of dopant in the polymer matrix [33, 34].

5 Dielectric studies

The variations of real part of permittivity (ϵ') as a function frequency for pure PANI and its nanocomposites (5, 10, 15, 20 and 25 wt% of ZnFe₂O₄ in PANI) is as shown in Fig. 6. It is observed that the permittivity value decreases with increase in the ZnFe₂O₄ weight percentages in PANI as well as applied frequency. However, the permittivity value decreases up to 15 wt% of ZnFe₂O₄ doping in PANI may be due to the dielectric relaxations, i.e., because of the movement of dipole and charge carriers due to the applied alternating field after which its value again increases. PANI, 20 and 25 wt% shows the high real permittivity (ϵ') as the molecular vibration or resonant electronic transition is much faster than relaxation mechanism this may be due to the blocking of charge carriers in between the interface or surface of the polymer back bone. This also may be effect the hopping mechanism in polymer nanocomposites due to increase in interface between the PANI and the fibers results high permittivity. The doping of the oxide fiber to its critical concentration may helps pinning of the polarons and bipolarons in small distance through the polymer chain is very easy and will get more conductivity with increasing in frequency [35]. The similar behaviour is observed in imaginary permittivity as shown in Fig. 7. However, the magnitude was found almost double and may be this anomalous change is due to the fiber structure of

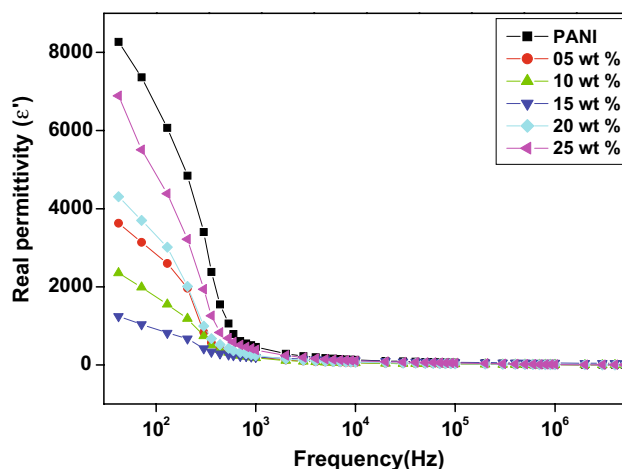


Fig. 6 Real part of permittivity as a function of applied frequency from 50 Hz to 5 MHz for 5, 10, 15, 20 and 25 wt% by doping ZnFe₂O₄ in polyaniline

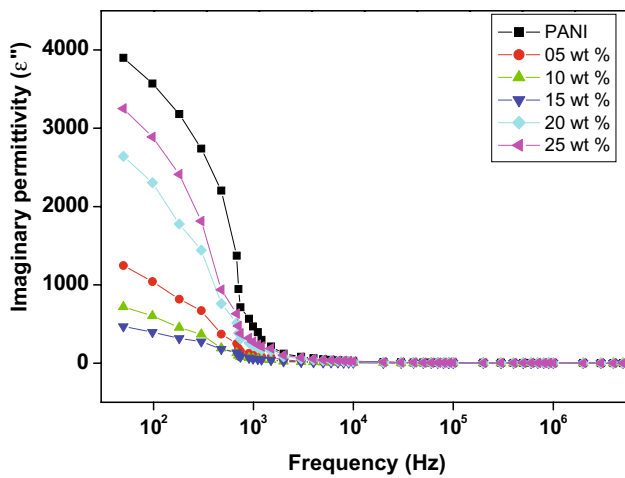


Fig. 7 Imaginary part of permittivity against frequency for PANI and PANI–ZnFe₂O₄ nanocomposites (5, 10, 15, 20 and 25 wt%) from 50 Hz to 5 MHz at room temperature

the nanocomposite which helps the charge carries to a long travel distance.

Figure 8 shows the variation of tangent loss as a function of applied frequency for pure PANI and its nanocomposites. It is observed that $\tan\delta$ decreases with respect to the applied frequency as well as the increase in fiber composition in the PANI. This is due to the decrease in the loss of energy due to the heating in the electrical circuit because of the change in between two fiber distance or between PANI and oxide fibers interface and agglomeration due to high energy surface of the nanofibers [36, 37]. The increase in the fiber concentration added the extra hopping site in between the two polymer fibers. Thus the tangent loss value

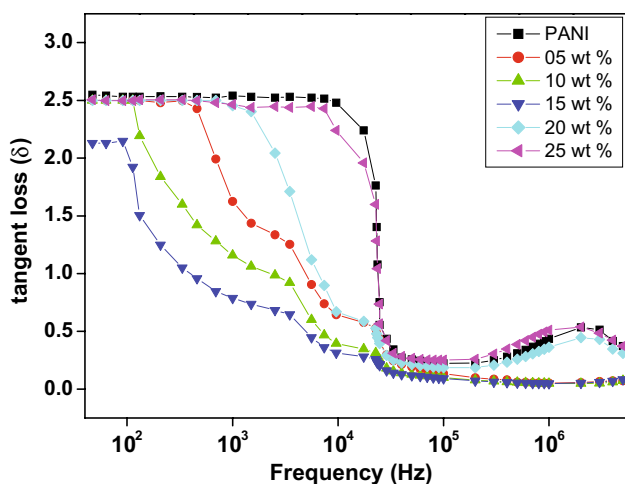


Fig. 8 Tangent loss as a function applied frequency for PANI and PANI–ZnFe₂O₄ nanocomposites (5, 10, 15, 20 and 25 wt%) at room temperature

decreases with increase in dopant in the matrix up to 15 wt%. At higher frequencies after 10⁴ Hz, these composites exhibit almost zero dielectric loss up to 15 wt% due to dominance in the tunneling phenomenon, i.e., the charge carriers move with in the interface of two nanocomposites fibers. Among all nanocomposites, 15 wt% shows low tangent value of 2.3 at lower frequency region and decreases to 0.131 with increase in initial frequency. Therefore, it is suggested that these composites can be used as lossless materials at frequencies beyond 10⁴ Hz [38, 39].

The Cole–Cole plots (Fig. 9) shows the variation of impedance as a function of frequency for various weight percentages of ZnFe₂O₄ nanofibers in PANI. It is found that the impedance value decreasing with increase in wt% of oxide fiber up to 15% may be due to decreasing in grain resistance and effect of bulk resistance because of grain boundaries together. It is also important to indicate that there are large dispersion in throughout applied frequency may be due to the combined effect of polarization mechanism, i.e., the dipole polarization and Maxwell–Wagner–Sillars polarization. This anomalous behaviour of the nanocomposites may be due to the fibers which run parallel to each other reducing the intra-distance between the two nanocomposites fibers. From the plot, it is found that a perfect semicircle arc is formed from the single origin at initial frequency due to the bulk resistance with series geometrical capacitance network. The formation of semi arc at the initial frequency suggest that not only bulk resistance plays a significant role but also that the relaxation mechanism equally effect the conduction mechanism of these PANI nanocomposites [40]. The trend of Nyquist profile clearly shows that there is a strong influence ZnFe₂O₄ fibers on conductivity of PANI. It also interesting to note that all the semicircles

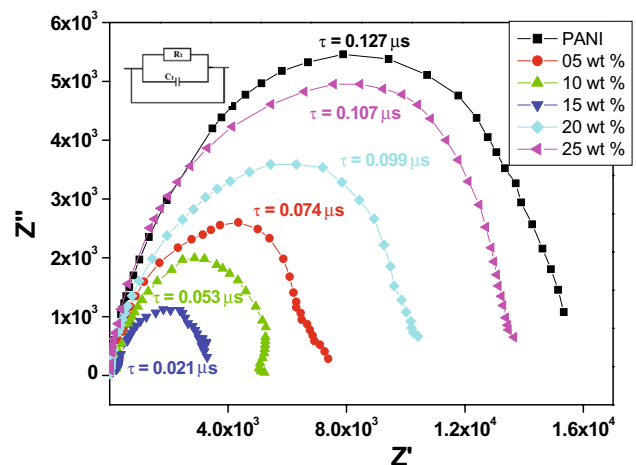


Fig. 9 Cole–Cole plot of PANI and 5, 10, 15, 20 and 25 wt% by doping ZnFe₂O₄ in polyaniline nanocomposites

arcs originate from a single point but the shape of the each graphs is different with the variation of ZnFe_2O_4 fibers in PANI which indicates that there will be a significant drift in the resistance of the nanocomposites. The substantial change in the Nyquist profile peaks is observed with variation of ZnFe_2O_4 in PANI. Therefore, it is owing that there will be a different relaxation time for each of the nanocomposites against frequencies. The relaxation time of ZnFe_2O_4 fibers doped PANI nanocomposites was calculated by taking a considering the maximum peak position of Cole–Cole plot at a particular frequency. It was found that the relaxation time decreases from 0.127 to 0.021 μs , with increases in ZnFe_2O_4 for 15 wt%. Among all nanocomposites, 15 wt% shows low bulk resistance because of the time taken for of relaxation is very small compare to other nanocomposites. This is due to the formation of series circuit with the oxide and PANI as shown in the inset figure. Therefore, these PANI nanocomposites have wide applications in technological field. However, these nanocomposites are good candidates compared to the earlier reported data [41, 42].

Figure 10 shows variation of ac conductivity for pure PANI and PANI/ ZnFe_2O_4 nanocomposites of various frequencies. The conductivity of pure PANI and its nanocomposites increases with increasing applied frequencies and obeys the universal power law [43, 44]. The conductivity is almost constant up to 10^4 Hz and then gradually increases with increasing in frequencies which are the characteristics of disordered amorphous materials. Among all composites 15 wt% shows high conductivity of 1.23 S/cm at 10^6 Hz due to hopping and tunneling of charge carriers and other nanocomposites show low conductivity because of blocking of charge carriers due o large interface and more granular distance between the two fibers.

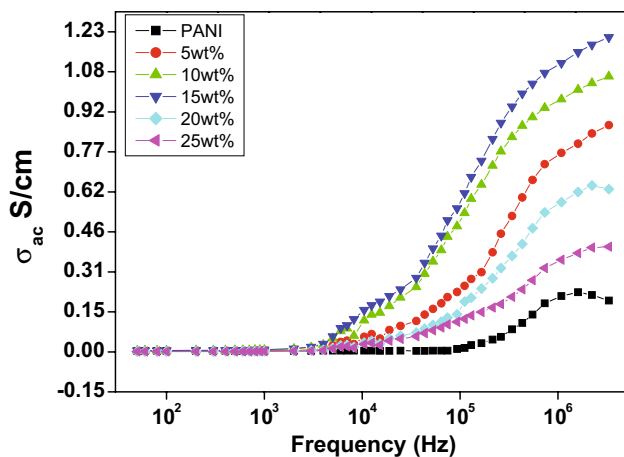


Fig. 10 AC conductivity of PANI and PANI– ZnFe_2O_4 nanocomposites (5, 10, 15, 20 and 25 wt%) at room temperature

6 Conclusion

The ZnFe_2O_4 fibers doped PANI nanocomposites have been synthesized by in situ oxidative polymerization technique. The prepared nanocomposites were characterized by FTIR and XRD analytical methods and characteristic peaks are observed for PANI and nanocomposites in the spectra confirm the formation of nanocomposites. The surface morphology was studied by using SEM and TEM and it was observed that the nanofibers were completely covered with PANI. The nanofibers help the nanocomposite nucleation in one-dimensions as a result a fiber like structure is formed. Among all nanocomposites, 15 wt% shows high conductivity of 0.35 S/cm having lowest activation energy and extending of polymer nanocomposites. Dielectric studies shows that the relative permittivity value almost doubles compare to imaginary part of permittivity with increase in applied frequency as well as the fiber. This anomalous behaviour observed due to shape of the oxide fiber which helps to grow in one-dimension. The conductivity of the 15 wt% nanocomposite shows high conductivity of 1.23 S/cm with lowest relaxation time of 0.021 μs . These nanocomposites can be used as loss less materials for electronic applications at higher frequency of 10^4 Hz. Therefore these composites are more suitable for engineering electronic applications.

References

1. R. Bavandpour, H.K. Maleh, M. Asif, V.K. Gupta, N. Atar, M. Abbasghorbani, *J. Mol. Liq.* **213**, 369 (2016)
2. H.K. Maleh, K. Ahanjan, M. Taghavi, M. Ghaemy, *Anal. Methods* **8**, 1780 (2016)
3. H.K. Maleh, F.T. Javazmi, A.A. Ensafi, R. Moradi, S. Mallakpour, H. Beitollahi, *Biosens. Bioelectron.* **60**, 1 (2014)
4. H.K. Maleh, P. Biparva, M. Hatami, *Biosens. Bioelectron.* **48**, 270 (2013)
5. M. Arshadi, M. Ghiaci, A.A. Ensafi, H. Karimi-Maleh, S.L. Suib, *J. Mol. Catal. A* **338**, 71 (2011)
6. H.K. Maleh, M. Hatami, R. Moradi, M.A. Khalilzadeh, S. Amiri, H. Sadeghifar, *Microchim. Acta* **183**, 2957 (2016)
7. S. Cheraghi, M.A. Taher, H.K. Maleh, R. Moradi, *J. Electrochem. Soc.* **164**, B60 (2017)
8. P. Singjai, A. Wongjamras, L.D. Yu, T. Tunkasiri, *Chem. Phys. Lett.* **366**, 51 (2002)
9. A. Varesano, C. Tonin, F. Ferrero, M. Stringhetta, *J. Therm. Anal. Calorim.* **94**, 55 (2008)
10. M.A.S.M. Yunos, A.T. Zainal, M.M.Y. Wan, *J. Chem. Eng. Mater. Sci.* **2**, 103 (2011)
11. P.A. Alivisatos, *Science* **271**, 933 (1996)
12. V.L. Kolvin, M.C. Schlamp, A.P. Alivisatos, *Nature* **370**, 353 (1994)
13. D.L. Klein, R. Roth, A.K.L. Lim, A.P. Alivisatos, *Nature* **389**, 699 (1997)
14. H.C. Pant, M.K. Patra, S.C. Negi, A. Bhatia, S.R. Vadera, N. Kumar, *Bull. Mater. Sci.* **29**, 379 (2006)

15. A.A. Syed, M.K. Dinesan, *Talanta* **38**, 815 (1991)
16. E.T. Kang, K.L. Neoh, *Prog. Polym. Sci.* **23**, 277 (1998)
17. N. Gospodinova, L. Terlemezyan, *Prog. Polym. Sci.* **23**, 1443 (1998)
18. D.C. Trivedi, in *Handbook of Organic Conductive Molecules and Polymers*, ed. by H.S. Nalwa, 2 edn. (Wiley, Chichester, 1997), p. 505
19. A.S. Roy, A. Parveen, K.R. Anilkumar, *J. Nanopart. Res.* **15**, 1337 (2013)
20. A. Parveen, A.S. Roy, Md. Shakeel, *Chem. Pap.* **67**, 350 (2013)
21. J. Stejskal, in *Dendrimers, Assemblies, Composite, MMLSeries 5*, ed. by R. Arshady, A. Guyot (Citius Books, London, 2002), p. 195
22. I. Sapurina, J. Stejskal, *Polym. Int.* **57**, 1295 (2008)
23. Y.J. Lin, Y.H. Chang, W.D. Yang, B.S. Tsai, *J. Noncryst. Solids* **352**, 789 (2006)
24. M.I. Baraton, G. Busca, M.C. Prieto, G. Ricchiardi, V.S. Escribano, *J. Solid State Chem.* **112**, 9 (1994)
25. T.S. Chao, W.M. Ku, H.C. Lin, D. Landheer, Y.Y. Wang, Y. Mori, *IEEE Trans. Electron Devices* **51**, 2200 (2004)
26. S.H. Chuang, M.L. Hsieh, S.C. Wu, H.C. Lin, T.S. Chao, T.H. Hou, *J. Am. Ceram. Soc.* **94**, 251 (2011)
27. A. Parveen, K.R. Anilkumar, A.S. Roy, *Sens. Lett.* **11**, 242 (2013)
28. A. Parveen, K.R. Anilkumar, A.S. Roy, *IEEE Sens. J.* **12**, 2817 (2012)
29. R. Patil, A.S. Roy, K.R. Anilkumar, S. Ekhelkar, *Ferroelectrics* **423**, 77 (2011)
30. Y.M. Kang, K.T. Kim, J.H. Kim, H.S. Kim, P.S. Lee, J.Y. Lee, H.K. Liu, S.X. Dou, *J. Power Sources* **133**, 252 (2004)
31. M. Lerch, W.Z. Laqua, *Anorg. Allg. Chem.* **610**, 57 (1992)
32. O. Yamamoto, Y. Takeda, R. Kanno, M. Noda, *Solid State Ion.* **22**, 241 (1987)
33. H. Obayashi, Y. Sakurai, T. Gejo, *J. Solid State Chem.* **17**, 299 (1976)
34. A.S. Roy, K.R. Anilkumar, M.V.N. Ambika Prasad, *J. Appl. Polym. Sci.* **121**, 675 (2011)
35. W. Xue, K. Fang, H. Qiu, J. Li, W. Mao, *Synth. Met.* **156**, 506 (2006)
36. A.S. Roy, K.R. Anilkumar, M.V.N. Ambika Prasad, *J. Appl. Polym. Sci.* **123**, 1928 (2012)
37. A.R. Phani, S. Santucki, *Mater. Lett.* **50**, 240 (2001)
38. A. Parveen, K.R. Anilkumar, S. Ekhelkar, M. Revansiddappa, M.V.N. Ambika Prasad, *Ferroelectrics* **377**, 63 (2008)
39. A.S. Roy, S. Gupta, S. Sindhu, A. Parveen, P.C. Ramamurthy, *Composites B* **47**, 314 (2013)
40. N. Dharmaraj, H.C. Park, C.K. Kim, H.Y. Kim, D.R. Lee, *Mater. Chem. Phys.* **87**, 5 (2004)
41. Z.D. Xiang, T. Chen, Z.M. Li, X.C. Bian, *Macromol. Mater. Eng.* **294**, 91 (2009)
42. Q. Li, W. Gao, P. Ma, *Adv. Nat. Sci.* **1**, 81 (2008)
43. G. Chakraborty, K. Gupta, A.K. Meikap, R. Babu, W.J. Blau, *J. Appl. Phys.* **109**, 033707 (2011)
44. A.S. Roy, S. Gupta, S. Sindhu, P.C. Ramamurthy, G. Madras, *Sci. Adv. Mater.* **6**, 946 (2014)